

Single-crystal neutron diffraction study of the magnetic structure of Er_3Co A. F. Gubkin,^{1,2} A. Podlesnyak,³ and N. V. Baranov^{1,4,*}¹*Ural State University, 620083 Ekaterinburg, Russia*²*Neutron Science Division, Korea Atomic Energy Research Institute, Daejeon 305-353, Republic of Korea*³*Spallation Neutron Source, Oak Ridge National Laboratory, Oak Ridge, Tennessee 37831, USA*⁴*Institute for Metal Physics, RAS, 620041 Ekaterinburg, Russia*

(Received 12 February 2010; published 13 July 2010)

The effect of the magnetic field applied along the main crystallographic directions on the magnetic structure of Er_3Co has been studied by means of single-crystal neutron diffraction technique. At zero field the compound exhibits a noncoplanar commensurate magnetic structure with ferromagnetic alignment of the Er magnetic-moment projections along the b axis in an orthorhombic unit cell. The present measurements revealed that the application of the magnetic field along the c direction [$c \perp (ab)$] leads to the pronounced metamagneticlike transition in the low-field region $\mu_0 H < 1.2$ T, although, the magnetization curve does not exhibit any anomalies. Combining the present single-crystal diffraction and magnetization data with the results of the previous powder neutron diffraction study [Gignoux *et al.*, *Solid State Commun.* **8**, 391 (1970)], we conclude that the nature of the magnetic ion, whether Kramers or non-Kramers, has a decisive effect on the commensurability of the magnetic structure of $R_3\text{Co}$. In particular, the commensurate magnetic structure observed in Er_3Co originate from the Kramers character of Er^{3+} ion in contrast to the incommensurate structures found earlier in $R_3\text{Co}$ with $R = \text{Tb}$ and Ho .

DOI: [10.1103/PhysRevB.82.012403](https://doi.org/10.1103/PhysRevB.82.012403)

PACS number(s): 75.30.Kz, 75.30.Gw, 61.05.F–

For more than three decades, the study of R_3T rare-earth (R) compounds with $3d$ metals ($T = \text{Co}, \text{Ni}$) has been a fascinating subject of condensed matter physics for their diversity of interesting properties, in particular, a variety of field-induced magnetic phase transitions, giant magnetoresistance, and complex magnetic phase diagrams.^{1–3} The R_3T compounds have the largest content of rare-earth metal within the $4f$ - $3d$ binaries and crystallize in the low-symmetry orthorhombic Fe_3C -type structure ($Pnma$ space group).⁴ Rare-earth atoms occupy two nonequivalent positions, $4c$ (R_{4c}) and $8d$ (R_{8d}). The atoms of $3d$ transition metal are located at the $4c$ position within the trigonal prisms formed by rare-earth atoms and do not possess any ordered magnetic moment.

Early investigations proposed that the R_3T compounds exhibit complex noncoplanar antiferromagnetic (AFM) or ferromagnetic structures which are commensurate with the crystal lattice. The presence of such structures was suggested to result from the competition between the Ruderman-Kittel-Kasuya-Yoshida exchange interaction and low-symmetry crystal electric field (CEF). However, more recent studies using new generation of neutron-scattering techniques have revealed that some of $R_3\text{Co}$ ($R = \text{Ho}, \text{Tb}$) compounds exhibit much more complex magnetic structures.^{5,6} The structures turn out to be incommensurate not only just below the magnetic ordering point but down to the lowest temperatures as well. We proposed recently that the non-Kramers character of the rare-earth ions is responsible for the incommensurability of the magnetic structures of these R_3T compounds at low temperatures.⁶

To our best knowledge, the only neutron powder diffraction study of the Er_3Co magnetic structure was done by Gignoux *et al.*¹ They found that the magnetic structure is commensurate (Er being a Kramers ion) and noncollinear with a ferromagnetic component along the b axis. Magnetic moments of Er ions in $4c$ sites are suggested to be aligned

strictly along the b direction, while in $8d$ positions the moments have a deviation from the b axis in such a manner that their projections along a and c axes are ordered antiferromagnetically. The magnetization measurements performed on single-crystalline samples of Er_3Co have revealed that this compound shows a ferromagneticlike behavior along the b axis in a low-field region.^{7,8} The magnetization does not saturate up to 12 T,⁸ which results apparently from a noncoplanarity of the magnetic structure. Along a and c directions smooth magnetization curves are observed with increasing external magnetic field without visible features which may be associated with transformations of the magnetic structure. However, the magnetoresistance measured along a and c axes exhibits some anomalies which were ascribed to the presence of the field-induced phase transitions in low fields $\mu_0 H \leq 1$ T.⁷

The main purpose of the present study is to assure the commensurability of the magnetic structure of Er_3Co to comprehend the role of Kramers-non-Kramers character of R ions in formation of various magnetic structures in the R_3T -type compounds and to achieve a better understanding of the magnetization process along main crystallographic directions. We present here single-crystal neutron diffraction study *proving* that Er_3Co indeed has a commensurate magnetic structure at ground state. Moreover, the measurements in the magnetic field $H \parallel c$ revealed the field-induced phase transition in low-field region.

The Er_3Co compound was obtained by arc melting in a helium atmosphere using erbium and cobalt of 99.9% and 99.99% purity, respectively. Single crystals were grown by the Bridgman technique in a resistive furnace. The phase purity of single crystals was checked by a metallographic method. The content of foreign phases was estimated to be less than 3%. The samples were cut along the main crystallographic directions $[100]$, $[010]$, and $[001]$ with dimensions of approximately $2.34 \times 2.62 \times 2.85$ mm³.

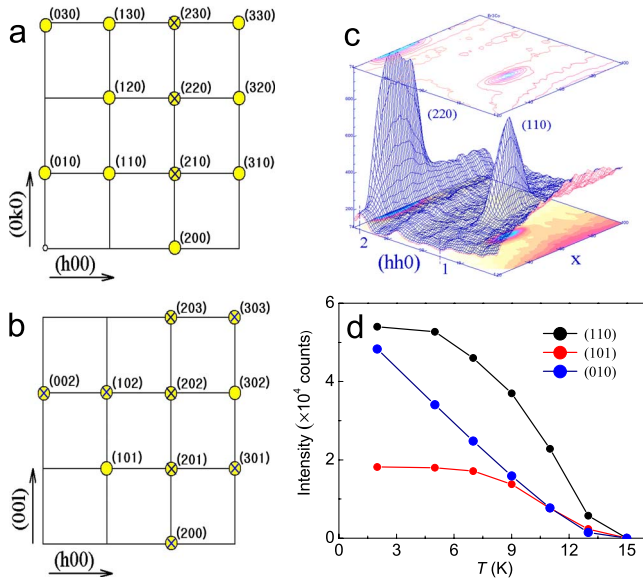


FIG. 1. (Color online) Schematic representations of the Bragg reflections measured at the temperature $T=2$ K in the $(hk0)$ [panel (a)] and $(h0l)$ [panel (b)] scattering plane. Crosses and circles correspond to nuclear and magnetic reflections, respectively. (c) The 3D visualization of the neutron-scattering intensity measured along $[hh0]$ direction in $(hk0)$ plane at $T=2$ K. (d) Temperature dependence of the integral intensity of (010) , (101) , and (110) magnetic reflections. The intensity of (010) reflection is reduced by four times.

Neutron diffraction measurements in external magnetic field were performed at the two-axis neutron diffractometer E4 installed in the research reactor BER II, the Helmholtz Center Berlin. The measurements were performed at temperatures from 2 K up to 30 K in vertical magnetic fields up to 6.5 T with wavelength of 2.44 Å. The analysis was done using Fullprof and SARAH programs.^{9,10} The dc magnetization was measured on the same sample along the main crystallographic directions by using a superconducting quantum interference device Magnetic Properties Measurement System magnetometer (Quantum Design, USA).

Let us discuss first zero-field magnetic structure. In order to check the commensurability of the magnetic structure and the model proposed by Gignoux *et al.*¹ we have performed the scans in $(hk0)$ and $(h0l)$ scattering planes in both the paramagnetic state at temperature $T=30$ K and in the magnetically ordered state at $T=2$ K. Figures 1(a) and 1(b) show the schematic representations of the measured nuclear and magnetic Bragg reflections in $(hk0)$ and $(h0l)$ scattering planes, respectively. An example of the three-dimensional (3D) visualization of the experimental scan along $[hh0]$ direction at $T=2$ K is displayed in Fig. 1(c). As shown in Fig. 1(d), the magnetic reflections appear at temperatures below 14 K. This critical temperature is well consistent with the Curie temperature $T_c \sim 13.8$ K derived from ac susceptibility, electrical resistivity, and specific-heat measurements.^{7,8} The magnetic scattering measured in $(hk0)$ and $(h0l)$ planes has revealed absence of any reflections with noninteger indexes which can be associated with the incommensurability of the magnetic structure. Thus, the determined zero-field

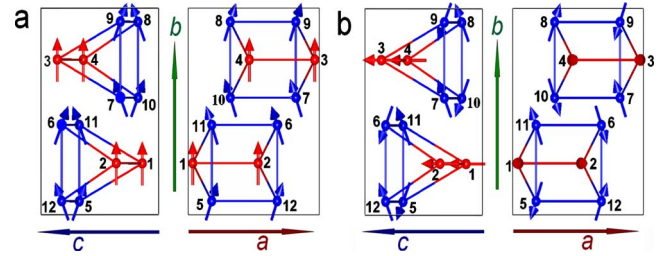


FIG. 2. (Color online) Schematic drawing of (a) zero-field and (b) field $H\parallel c$ magnetic structures in Er_3Co .

magnetic structure (schematically shown in Fig. 2) is consistent with a model of the commensurate noncollinear ferromagnetic structure suggested in Ref. 1. The commensurate magnetic structures (although, different from Er_3Co case) were also found in other $R_3\text{Co}$ compounds with Kramers-type ions, $R=\text{Dy}$ and Nd .^{3,11} This is in contrast to the incommensurate magnetic structure established for the systems with non-Kramers rare earth, e.g., Ho_3Co and Tb_3Co .^{5,6} The type of the magnetic structure within $R_3\text{Co}$ series can be understood on the base of the periodic field model which takes into account the periodic exchange field and CEF effects.¹² According to this model an incommensurate magnetic structure may be observed down to low temperatures when a non-Kramers R^{3+} ion has a nonmagnetic singlet ground state due to splitting of the multiplet by low-symmetry CEF. It should be noted that the specific-heat measurements and calculations of the crystal-field effects performed for Er_3Co by Saito *et al.*¹³ have shown that the crystal field and the exchange field are of the same order of magnitude. Below the Curie temperature $T_c=13.8$ K, the main contribution to the magnetic part of the entropy in Er_3Co is associated with the low-lying doublet.⁷

Let us turn to the field-induced magnetic structures. In order to reveal difference in the magnetization process along main crystallographic directions we have performed the neutron-scattering measurements in $(h0l)$ and $(hk0)$ planes with magnetic field applied along b and c directions, respectively. The schematic representations of the Bragg reflections observed at 6.5 T are displayed in Figs. 3(a) and 3(b). As expected, the magnetic field applied along the easy b direction does not affect the Bragg reflections in comparison with zero-field picture [compare Fig. 3(a) with Fig. 1(a)] while the application of a magnetic field along the c direction leads to substantial changes in the neutron scattering. The magnetic reflections of the $(0k0)$ type with odd k which were well pronounced in zero field, are observed to disappear under application of the magnetic field along the c direction $\mu_0 H = 6.5$ T. Furthermore, the reflections with even k [i.e., (020) , (040) , and (060)] which have zero intensities at $H=0$ are found to appear in a field-induced state. In order to reveal the evolution of the magnetic state of Er_3Co the intensities of several magnetic reflections were measured as a function of the external magnetic field. As follows from Fig. 3(c), the integral intensity of reflections (101) and (001) remains almost constant under magnetic field applied along the b axis while the application of the magnetic field along the c direction changes the intensities of (010) and (110) dramatically.

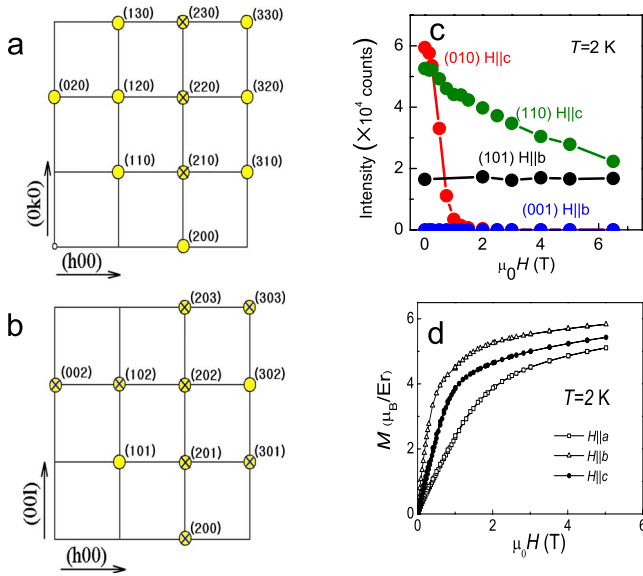


FIG. 3. (Color online) (a) The schematic representations of Bragg reflections measured at $T=2$ K in the $(hk0)$ plane in the magnetic field 6.5 T applied along the b direction (a) and in the $(h0l)$ plane in the field 6.5 T applied along c direction (b). Crosses and circles correspond to nuclear and magnetic reflections, respectively. (c) The integral intensity of some magnetic reflections versus magnetic field applied along different axes as labeled. The intensity of (010) reflection is reduced by four times. (d) Field dependencies of the magnetization measured along the main crystallographic directions of the single crystal Er_3Co at $T=2$ K.

The integral intensity of the (110) decreases gradually with increasing field up to 6.5 T. The intensity of the (010) magnetic reflection goes rapidly down to zero in relatively weak magnetic field $\mu_0 H \leq 1.2$ T, which is indicative of the metamagnetic phase transition from the antiferromagnetic to ferromagnetic alignment of the projections of Er magnetic moments onto the c axis. With further increase in the magnetic field, Er magnetic moments rotate in the direction of the applied field. These results are in agreement with the behavior of the magnetoresistance measured along different axes of Er_3Co . As was shown in Ref. 7 the application of a magnetic field along the c axis leads to the sharp fall (by about 7%) of the magnetoresistance in the same field interval while along the easy b axis, the insignificant change in the magnetoresistance (less than 0.5%) was observed in fields up to 1.5 T. According to the periodic field model, the application of a magnetic field at low temperatures may lead to the phase transition from a commensurate to incommensurate structure in the case of non-Kramers R ions. However, our single-crystal neutron diffraction measurements show that the magnetic structure of Er_3Co remains commensurate under application of a magnetic field up to 6.5 T (see Fig. 3). In our opinion, this is because of Kramers character of Er^{3+} ions. The shape of the magnetization curves measured along the different axes of Er_3Co does not allow one to distinguish the metamagnetic behavior [Fig. 3(d)]. The $M(H)$ dependencies measured along the a and c axes at $T=2$ K do not exhibit any visible features that is in agreement with previously reported results in Refs. 7 and 8. Bearing in mind the data

obtained for other metamagnetic materials¹⁴ an absence of distinct indications on the metamagneticlike transitions in the magnetization measurements along a and c axes may be associated with the superposition of several contributions to the magnetization change in the same field interval. The magnetic structure of Er_3Co implies an incoherent behavior of Er_{4c} and Er_{8d} moments under application of a low magnetic field along c or a axis. Owing to the combination of spin-flip processes within subsystem of Er_{8d} moments and the rotation of Er_{4c} moments such a magnetization process cannot be described as a simple spin-flip transition or spin-reorientation transition. The increase in the field along c or a axis results apparently not only in the appearance of the nuclei of a new field-induced phase and the growth of the volume of nuclei via domain (interphase) wall motion as in other metamagnets,¹⁴ but simultaneously leads to increase in the magnetization within nuclei.

The nearly constant values of the intensity of magnetic Bragg peaks in the field applied along the b axis implies that the increase in the magnetization in this direction is not accompanied by substantial changes in the magnetic structure unlike the c direction. In a low-field region, the magnetization process along the easy b direction occurs apparently via domain-wall movement as in conventional ferromagnet. We did not make the neutron diffraction measurements in the field applied along the a direction. However, bearing in mind zero-field picture (see Fig. 2), i.e., the presence of AFM alignment of projections of the magnetic moment onto axis a , as well as the magnetoresistance data,⁷ one can suggest that the magnetization process would be similar to the $H||c$ case.

In order to confirm the suggestion about the field-induced spin-flip transition along the c axis it is important to classify the possible spin configurations in terms of the representational analysis. The Er_3Co space group $Pnma$ consists of eight symmetry operations which leave the propagation vector $k=(000)$ invariant. Thus the little group \mathcal{G}_k has eight associated irreducible representations which can be found in Kovalev tables¹⁵ or calculated directly by means of SARAH program.⁹ The decomposition of the magnetic representation of the space group $Pnma$ with $k=(000)$ for Er 4c and 8d sites is given by $\Gamma_{\text{MAG}}^{4c} = \Gamma_1^{(1)} + 2\Gamma_2^{(1)} + 2\Gamma_3^{(1)} + \Gamma_4^{(1)} + \Gamma_5^{(1)} + 2\Gamma_6^{(1)} + 2\Gamma_7^{(1)} + \Gamma_8^{(1)}$; $\Gamma_{\text{MAG}}^{8d} = 3\Gamma_1^{(1)} + 3\Gamma_2^{(1)} + 3\Gamma_3^{(1)} + 3\Gamma_4^{(1)} + 3\Gamma_5^{(1)} + 3\Gamma_6^{(1)} + 3\Gamma_7^{(1)} + 3\Gamma_8^{(1)}$, respectively. The basis vectors associated with the irreducible representation for 4c and 8d atomic sites are summarized in Table I. An analysis of the basis vectors combinations revealed the magnetic state with the ferromagnetic arrangement of projections of Er magnetic moments along b or c direction (zero-field or field-induced magnetic state) can exist in case of irreducible representations Γ_5 and Γ_7 , respectively. As one can see from the Table I, the ferromagnetic structure (Γ_7) with the resultant moment along the c axis may be obtained from the initial ferromagnetic structure (Γ_5) with the net moment along the b axis by spin-flip processes occurring for some Er magnetic moments under influence of the magnetic field. The simulation of the magnetic structure induced by the application of the magnetic field along the c axis shows the presence of a nonzero intensity of $(0k0)$ reflections with even k and zero intensity of the reflections with odd k , which is in agreement with our neutron diffrac-

TABLE I. Basis vectors for Er atoms in 4c and 8d sites for two spin configurations, zero-field (Γ_5) and field-induced (Γ_7) states. The irreducible representations and the propagation vector follow those of Ref. 15. Atom numbers correspond to that in Figs. 2(a) and 2(b).

IR	BV	Basis vector components for 4c sites			
		1	2	3	4
(Γ_5)	ψ_1	0 2 0	0 2 0	0 2 0	0 2 0
(Γ_7)	ψ_1	2 0 0	$\bar{2}$ 0 0	2 0 0	$\bar{2}$ 0 0
	ψ_2	0 0 2	0 0 2	0 0 2	0 0 2
		Basis vector components for 8d sites			
		5, 9	6, 10	7, 11	8, 12
(Γ_5)	ψ_1	1 0 0	$\bar{1}$ 0 0	$\bar{1}$ 0 0	1 0 0
	ψ_2	1 0 0	$\bar{1}$ 0 0	$\bar{1}$ 0 0	1 0 0
	$-\psi_3$	0 1 0	0 1 0	0 1 0	0 1 0
(Γ_7)	$-\psi_1$	1 0 0	$\bar{1}$ 0 0	1 0 0	$\bar{1}$ 0 0
	$-\psi_2$	0 1 0	0 1 0	0 $\bar{1}$ 0	0 $\bar{1}$ 0
	ψ_3	0 0 1	0 0 1	0 0 1	0 0 1

tion data obtained in the external magnetic field.

In summary, single-crystal neutron diffraction in magnetic fields together with magnetization measurements have been performed for the study of the peculiarities of the magnetization processes along different crystallographic directions of Er_3Co . Our study proves that the ground state of Er_3Co is noncoplanar ferromagnet with commensurate magnetic structure [propagation vector $k=(000)$]. Bearing in mind the data obtained for other $R_3\text{Co}$ compounds with non-Kramers (Ho and Tb) (Refs. 5 and 6) and Kramers (Dy and Nd) (Refs. 3 and 11) ions the results obtained in the present work support the suggestion about the non-Kramers character of the rare-earth ions as a key factor determining the incommensurability of the magnetic structure of R_3T compounds at low temperature. Despite an absence of visible features on magnetization curves measured along b and c axes of the Er_3Co

single crystal, the neutron diffraction measurements performed under application of a magnetic field have revealed a substantial difference in the magnetization process along these axes. Unlike the easy b axis along which the increase in the magnetic field does not change substantially the neutron scattering, the magnetic field ~ 1.2 T applied along the c axes is found to lead to a metamagneticlike transition from the antiferromagnetic alignment of magnetic-moment projections to the ferromagnetic one. The magnetization process along the a axis is suggested to be analogous to that observed along the c direction.

The present work was partly supported by the Program of the Presidium RAS (Project No. 09-P-1008). ORNL is managed by UT-Battelle, LLC, under Contract No. DE-AC05-00OR22725 for the U.S. Department of Energy.

*Corresponding author; nikolai.baranov@usu.ru

¹D. Gignoux, R. Lemaire, and D. Paccard, *Solid State Commun.* **8**, 391 (1970).

²G. Primavesi and K. N. R. Taylor, *J. Phys. F: Met. Phys.* **2**, 761 (1972).

³N. V. Baranov, A. N. Pirogov, and A. E. Teplykh, *J. Alloys Compd.* **226**, 70 (1995).

⁴K. H. J. Buschow and A. S. van der Goot, *J. Less-Common Met.* **18**, 309 (1969).

⁵A. Podlesnyak, A. Daoud-Aladine, O. Zaharko, P. Markin, and N. Baranov, *J. Magn. Magn. Mater.* **272-276**, 565 (2004).

⁶N. V. Baranov, A. F. Gubkin, A. P. Vokhmyanin, A. N. Pirogov, A. Podlesnyak, L. Keller, N. V. Mushnikov, and M. I. Bartashevich, *J. Phys.: Condens. Matter* **19**, 326213 (2007).

⁷N. V. Baranov, G. Hilscher, A. V. Korolev, P. E. Markin, H. Michor, and A. A. Yermakov, *Physica B* **324**, 179 (2002).

⁸N. V. Tristan, S. A. Nikitin, T. Palewski, and K. Skokov, *J. Magn. Magn. Mater.* **251**, 155 (2002).

⁹<http://www.chem.ucl.ac.uk/people/wills/index.html>

¹⁰J. Rodríguez-Carvajal, *Physica B* **192**, 55 (1993).

¹¹Y. Adachi, Y. Lu, I. Umehara, and K. Sato, *J. Appl. Phys.* **85**, 4750 (1999).

¹²D. Gignoux and D. Schmitt, *Phys. Rev. B* **48**, 12682 (1993).

¹³A. Saito, A. Tutai, M. Sahashi, and T. Hashimoto, *Jpn. J. Appl. Phys., Part 2* **34**, L171 (1995).

¹⁴E. Stryjewski and N. Giordano, *Adv. Phys.* **26**, 487 (1977).

¹⁵O. V. Kovalev, *Representation of Crystallographic Space Groups* (Gordon and Breach, Switzerland, 1993).